Cement & Concrete Composites 32 (2010) 639–648

Contents lists available at ScienceDirect

Cement & Concrete Composites

journal homepage: www.elsevier.com/locate/cemconcomp

Mechanical properties of reactive powder concrete containing high volumes of ground granulated blast furnace slag

Halit Yazıcı *, Mert Y. Yardımcı, Hüseyin Yiğiter, Serdar Aydın, Selçuk Türkel

Department of Civil Engineering, Engineering Faculty, Dokuz Eylül University, Buca 35160, İzmir, Turkey

ARTICLE INFO

Article history:
Received 26 April 2007
Received in revised form 7 June 2010
Accepted 8 July 2010
Available online 14 July 2010

Keywords:
GGBFS
RPC
Autoclave
Steam curing
Fracture energy

ABSTRACT

The mechanical properties (flexural strength, compressive strength, toughness and fracture energy) of steel microfiber reinforced reactive powder concrete (RPC) were investigated under different curing conditions (standard, autoclave and steam curing). Portland cement was replaced with ground granulated blast furnace slag (GGBFS) at 20%, 40% and 60%. Sintered bauxite, granite and quartz were used as aggregates in different series. The compressive strength of high volume GGBFS RPC was over 250 MPa after autoclaving. When an external pressure was applied during setting and hardening stages, compressive strength reached up to 400 MPa. The amount of silica fume can be decreased with increasing amount of GGBFS. SEM micrographs revealed the tobermorite after autoclave curing.

1. Introduction

Reactive powder concrete (RPC) is a relatively new cement-based material developed through micro-structural engineering. Conventional RPC is composed of cement and ultra-fine powders, such as crushed quartz and silica fume; it also has low water content (water/cementitious ratio generally lower than 0.20). A highly dense matrix is achieved by optimizing the granular packing of these powders [1]. The basic principles for the development of RPC have been explained by the Richard and Cheyrezy [2]. As compared to ordinary cement-based materials, the primary improvements of RPC are related to particle size homogeneity, porosity, and microstructures. The mechanical properties that can be achieved include compressive strength in the range between 200 and 800 MPa, fracture energy in the range between 1200 and 40,000 J/m^2, and ultimate tensile strain on the order of 1% [1,2]. This is generally achieved by a micro-structural engineering approach, including elimination of the coarse aggregates, reducing the water-to-cementitious material ratio, lowering the $CaO–SiO_2$ ratio by introducing silica components, and incorporation of steel micro-fibers [1–3]. Nowadays, RPC is regarded as a promising material for special prestressed and precast concrete members, including those within industrial and nuclear waste storage facilities [2–5]. Although production costs of RPC are generally high, some economical advantages also exist in RPC applications. It is possible to reduce or eliminate passive reinforcement using steel fibers. And, due to ultra-high mechanical performance of RPC, the thickness of concrete elements can be reduced, which results in materials and cost savings.

Ground granulated blast furnace slag (GGBFS) has been used for many years as a supplementary cementitious material in concrete technology. The slag is a by-product material obtained from the manufacture of pig iron in the blast furnace and is formed by the combination of earthy constituents of iron ore with limestone flux. Due to its pozzolanic nature, GGBFS is a beneficial mineral admixture for concrete. It reduces the porosity, the pores become finer, and the change in mineralogy of the cement hydrates leads to a reduction in mobility of chloride ions [6].

Cement dosage of RPC is generally over 800–1000 kg/m^3. A high amount of cement not only affects the production costs, but also has negative effects on the heat of hydration and may cause shrinkage problems. Replacing cement with mineral admixtures seems to be a feasible solution to these problems. Furthermore, incorporation of mineral admixtures may positively affect the durability of concrete. Wang and Zhi [7] showed that the maximum heat of cement hydration in binary/ternary cement (fly ash and/or GGBFS) concrete decreased with supplementary cementitious material (SCM) replacements, as a result, SCM concrete generally has a lower risk of thermal cracking than Portland cement (PC) concrete. Furthermore, the pore structure of concrete with GGBFS is drastically altered and GGBFS can contribute significantly to the reduction of corrosion risk by increasing the resistivity of concrete [6,8]. Detwiler et al. [9] investigated the effectiveness of using SCM to increase the chloride penetration resistance of accelerated cured concrete and found that SCM concretes performed better

* Corresponding author. Tel.: +90 232 4127044; fax: +90 232 4127253.
E-mail address: halit.yazici@deu.edu.tr (H. Yazıcı).

0958-9465/$ - see front matter © 2010 Elsevier Ltd. All rights reserved.
doi:10.1016/j.cemconcomp.2010.07.005

than PC concretes. In addition, chloride penetration resistance of PC concrete is adversely affected by accelerated curing. However, with the use of the ternary ordinary PC–SF–GGBFS binders, accelerated curing did not have detrimental effects on chloride penetration resistance [10].

Original reactive powder concrete – in the form of a superplasticized cement mixture with silica fume, steel fibers and ground fine quartz (150–400 μm) – was studied by Collepardi et al. [11] in comparison with a modified RPC where a graded natural aggregate (max size 8 mm) was used to replace the fine sand and/or part of the cementitious binder. The latter performed better, in terms of higher strength and lower drying shrinkage or creep strain.

Massidda et al. [12] studied the effects of autoclaving under saturated vapor at 180 °C on the physical and mechanical properties of reactive-powder mortars reinforced with brass coated steel fibers. Autoclaving generally produced beneficial effects on flexural and compressive strength. High pressure steam curing for 3 h of specimens pre-cured at ambient temperature for 3 days, yielded flexural strength of 30 MPa and compressive strength of 200 MPa. Shaheen and Shrive [13] investigated freeze–thaw resistance of RPC. Their results showed that RPC have excellent resistance with no sign of damage up to 600 cycles according to ASTM C 666 test procedure. Talebinejad et al. [14] investigated the mechanical properties of RPC containing Portland cement and SF. Compressive strength of 230 MPa was achieved following with the different curing methods (20 °C water + 90 °C water); however, the cement content was as high as 1900 kg/m^3. Ma et al. [15] used crushed basalt in the production of ultra-high performance concrete (UHPC). It was shown that mixtures having particle size from 2 to 5 mm exhibited similar mechanical performance compared to the RPC in which the maximum size of aggregate was smaller than 1 mm. Rougeau and Borys [16] showed that UHPC can be produced with fine particles other than SF such as fly ash, limestone microfiller or metakaolin. Jooss and Reinhardt [17] showed that permeability and diffusion coefficient of high performance concrete (HPC) and RPC were much lower than conventional waterproof concrete according to DIN 1045. Moreover, these coefficients were much lower in RPC than HPC.

The presence of secondary materials affects the cement reactivity [18]. The hydration of the cement in pastes containing slag was first retarded and then enhanced at some later age. Secondary materials form additional hydration products. This effect was shown by the additional combined water per unit mass of Portland cement in the blended mixtures and by the depletion of calcium hydroxide [18]. Slag depleting the calcium hydroxide also used it as an activator and the additional hydrate produced increased the quantity of combined water significantly [18,19]. The hydration of slag cement was investigated by the Escalante-Garcia and Sharp [20] and the hydration of alite was greatly increased from very early stages by the presence of GGBFS [20]. For the slag cement, there was marked temperature dependence and the curves were similar to those of the neat cement, except that hydration was faster. The peak contents of CH in the pozzolanic cements shifted to shorter times and lower values as the temperature was increased, indicating that the pozzolanic reaction was favored by the higher temperatures. The lower CH content at 60 °C in the slag blend may indicate a stronger pozzolanic behavior of the slag in the early stages of hydration [20]. Gutteridge and Dalziel [21] also showed that the presence of a fine, non-hydraulic filler also significantly enhanced the hydration of the Portland cement.

In this study, the effects of curing conditions and high volume GGBFS replacement on the mechanical properties of steel microfiber reinforced RPC are investigated. Cement is replaced with GGBFS at different proportions. SF is used as a silica source to decrease the $CaO–SiO_2$ ratio in the binder system, to react with CH, to fill micro level pores and to convert the α-C_2SH to tobermorite-like ($C_5S_6H_5$) structures under autoclave curing. Test results are presented comparatively with a control mix, which has only cement and SF as a binder.

2. Experimental program

Sintered bauxite (0–1 and 1–3 mm), granite (1–3 mm) and quartz (0–0.4 and 0.5–1.0 mm) were used as aggregates. Specific gravities of 1–3 mm bauxite, 1–3 mm granite and 0.5–1.0 mm quartz were 3.24, 2.62 and 2.65, respectively. A polycarboxylate based superplasticizer (SP) in conformity with ASTM C 494 was used. The physical, chemical and mechanical properties of Portland cement (CEM I 42,5), properties of silica fume and slag are presented in Table 1. Brass coated steel fibers with 6 mm length and a diameter of 0.15 mm were used; the aspect ratio and tensile strength of the fibers were 40 and 2250 MPa, respectively.

Mixture designs are given in Table 2. According to GGBFS and bauxite contents, the mixtures were abbreviated as B-S20, B-S40, B-S60, while granite incorporated mixtures were abbreviated as G-S20, G-S40, G-S60. Moreover, B-S0 and G-S0 represent control mixtures that contain only cement and SF as a binder without GGBFS.

The mixtures were combined in a high-speed mixer (470 rpm) and compacted by hand operations and vibration. Dry powders and aggregates were mixed at low speed for about 1 min. After the water addition, the concrete was mixed at low and high speeds for about 2 min. SP was added to premixed material and mixed at high speed for about 5 min. Finally, steel fibers were added and mixed at high speed for about 2 min. Because of the high binder volume, very low water/binder ratio and high SF content, the mixtures could not be compacted by only vibration. The specimens were kept in the moulds for 16 h at room temperature of 20 °C. After demolding, one group the specimens was exposed to steam curing (SC) at 100 °C for seven days, heating rate was of 11 °C/h; another group was autoclaved (AC) at 210 °C under 2.0 MPa pressure for 8 h. Maximum temperature and maximum pressure were reached in 2.5 h. The remaining specimens were cured in standard conditions (STD, water curing at 20 °C). The specimens, which were subjected to heat treatment, were kept in laboratory atmosphere for cooling after completion of their curing periods.

Notched prismatic specimens (75 × 75 × 305 mm) were used to determine the flexural strength, fracture energy and toughness according to RILEM Technical Committee 50-FMC guidelines. Flexural specimens were tested at a loading rate of 0.1 mm/min up to mid-span deflection of 3.0 mm under a closed-loop control test procedure. The specimens were loaded from their mid-span and the clear distance between simple supports was 270 mm. The beam specimens had the same notch depth for all series, equal to half of the beam height. The fracture energy and toughness were determined from the load–displacement curves of the three point bending test results. Fracture energy was calculated according to

$$G_F = \frac{W + mg\delta(L'/L)}{A_{net}} \quad (1)$$

where W is area under the load–deflection curve up to 3 mm, m is mass of the beam, g is the acceleration due to gravity, δ is the deflection of the beam, L and L' are length and span length of the beam and A_{net} is the net cross-sectional area of the beam.

Three notched beams were used for the flexural test of each material combination and average values were reported. The standard deviation for flexural strength was between 2.1 and 3.6 MPa according to the different mixtures. The compressive strength test was performed following the flexural tests. The two broken pieces left from flexural test were subjected to compressive strength test according to the ASTM C 116 and BS1881. Thus, the average of six

Table 1
Physical, chemical and mechanical properties of cement, silica fume and slag.

	Chemical composition (%)			Physical properties of cement	
	Cement (PC)	Silica Fume (SF)	Slag (GGBFS)		
SiO_2	20.1	92.26	39.66	Specific gravity	3.13
Al_2O_3	5.62	0.89	12.94	Initial setting time (min)	130
Fe_2O_3	2.17	1.97	1.58	Final setting time (min)	210
CaO	62.92	0.49	34.20	Volume expansion (mm)	1.00
MgO	1.14	0.96	6.94	Specific surface	
Na_2O	0.30	0.42	0.20	Cement (m^2/kg) Blaine	380
K_2O	0.85	1.31	1.44	SF (m^2/kg) Nitrogen absorption	20,000
SO_3	2.92	0.33	0.72	GGBFS (m^2/kg) Blaine	396
Cl^-	0.0096	0.09	–	Compressive strength of cement (MPa)	
Loss on ignition	3.84	–	1.20	2 days	29.9
Insoluble residue	0.63	–	–	7 days	43.2
Free CaO (%)	0.52	–	–	28 days	51.9

Table 2
Composition of the mixtures.

Material (kg/m^3)	Bauxite				Granite			
	B-S0	B-S20	B-S40	B-S60	G-S0	G-S20	G-S40	G-S60
Cement	940	752	564	376	940	752	564	376
SF	282	282	282	282	282	226	169	113
GGBFS	0	188	376	564		188	376	564
1–3 mm Bauxite	940	922	904	887	–	–	–	–
0–1 mm Bauxite	240	236	233	227	–	–	–	–
1–3 mm Granite	–	–	–	–	800	840	881	921
0.5–1 mm Quartz	–	–	–	–	100	104	109	114
0–0.4 mm Quartz	–	–	–	–	100	104	109	114
Water	125	125	125	125	125	125	125	125
Steel fiber	234	234	234	234	234	234	234	234
SP (L/m^3)	55	55	55	55	61	52.0	44.0	37.0
Water from SP (L/m^3)	33	33	33	33	37	31	26	22
Water*/cement	0.17	0.21	0.28	0.42	0.17	0.21	0.27	0.39
Water/powder	0.10	0.10	0.10	0.10	0.10	0.11	0.11	0.12
Water*/powder	0.13	0.13	0.13	0,13	0.13	0.13	0.14	0.14

* Calculated as total water (water + water from SP)/powder ratio.

specimens was used to evaluate compressive strength of the mixtures. On the other hand, flexural load–deflection curves were drawn using the result closest to the average mechanical performance. The mechanical tests were carried out at the ages of 7, 28 and 90 days after STD curing. Testing age of SC and AC cured specimens were 8 and 2 days, respectively.

3. Results and discussion

3.1. Influence of the blast furnace slag content on compressive strength of RPC

The compressive strength of mixtures containing bauxite aggregate cured under different conditions is presented in Fig. 1. The compressive strengths of B-S0, B-S20, B-S40 and B-S60 mixtures are 285, 298, 277 and 251 MPa after autoclave curing, respectively. These values are 199, 208, 199 and 191 MPa for 28-day water curing. It can be seen that, although autoclaving and steam curing improved the compressive strength considerably, 28-day standard curing may also be sufficient to reach 200 MPa compressive strength. Note that the age of SC and AC cured specimens were 8 and 2 days, respectively. Compared to the control mixture (B-S0), 20% GGBFS replacement slightly increased the compressive strength, 40% GGBFS maintained the compressive strength close to the control mixture, and 60% GGBFS slightly reduced the compressive strength. This finding is valid for all curing conditions except for 7-day standard water curing in which 40% and 60% GGBFS

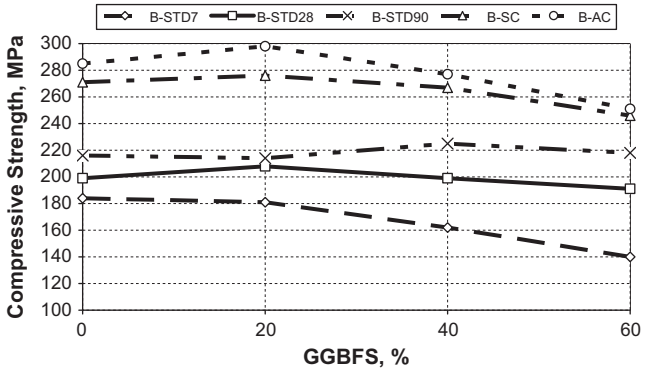

Fig. 1. The influence of GGBFS content on compressive strength of Bauxite aggregate RPC (STD: Standard curing, SC: Steam curing, AC: Autoclave curing).

replacement caused some reduction in compressive strength. Yazıcı [23] also reported that high volume GGBFS or fly ash can be used in ultra-high strength concrete. Although there were no steel fibers, compressive strength reached 185 MPa after autoclaving for 40% GGBFS replacement at similar PC contents (850 kg/m^3) with this study [23]. The beneficial effects of GGBFS in concrete results from the modified microstructure of the cementitious paste, which has more capillary pores filled with low density C–S–H gel than Portland cement paste [24,25]. GGBFS can be effectively used

to reduce the pore sizes and cumulative pore volume of the paste [26]. The hydration mechanism of GGBFS is different from that of cement, which was investigated by Escalante-Garcia [19]. The strength development of slag cements is slow at low temperatures and favored by high temperatures according to that research. The pozzolanic reaction is also favored by increased hydration temperatures. Non evaporable water (NEW) values for the slag blend were clearly higher than those of the corresponding neat cement fraction, probably due to the hydraulic reactions of the slag. Thus, the increased NEW values observed in the blended cements are probably due to the combined effects of an enhanced cement hydration and to a contribution from the reactions of the replacement materials [19]. The C–S–H formed in slag cement hydrated at 25 °C has CaO/SiO_2 ratio of 1.61–1.79 [26–29]. Normally RPC has high cement content and very low water/binder ratio, which causes rapid hydration reaction, high heat of hydration and shrinkage. These negative properties can be removed by using the GGBFS. It is well known that steam curing at 65–85 °C for 3–12 h normally causes ultimate strength reduction for neat Portland cement. This is explained by the increased porosity of the hydrated paste by rapid formation of dense hydration products around the cement grains which retards further hydration and strength development [19]. The development of microstructure and compressive strength of blended cement pastes hydrated at temperatures raging from 10 °C to 60 °C was investigated by Escalante-Garcia and Sharp [22]. According to this study the only blended cement paste that had substantially improved strength compared with the neat cement paste was that containing blast furnace slag, especially at 60 °C. The blended cement paste cured at 60 °C showed similar initial values to that of neat cement pastes and after a year it had reached higher values. Although there was some evidence for high temperature inversion in the blended cement pastes it was not as marked as in the neat cement pastes [22].

In this study, the compressive strength of all steam cured specimens was greater than that of 28-day or 90-day standard cured specimens in water. This can be explained by prolonged steam curing at 100 °C which possibly caused the extended pozzolanic reactions. Therefore, the reactivity of the binder phases increased by elevated temperatures which also increased the compressive strength of all mixtures. Note that control mixture also showed similar behavior compared to the GGBFS mixtures. This can be attributed to the significant amount of SF in the control mixture. These findings are also accordance with previous studies [30,31]. SF is one of the most reactive pozzolanic materials in view of its ultrafine particle size and high surface area. GGBFS is also a hydraulic material, i.e. reacts with water but in a slow manner [20], much slower than SF. However, both materials benefit greatly from thermal activation, perhaps more markedly the slag [19,20]. The presence of secondary materials also affects the cement reactivity [18,21,22]. For example, under high temperature curing conditions (or during the heating stage), PC reacts yielding CH; the CH will react first with GGBFS or SF. CH consumption will accelerate the PC reactions, which will consume more water and form more CH, which will in turn react with SF and GGBFS. In other words, there are many reactive components in RPC mixtures some part of which may remain unreacted after standard curing. Autoclaving or steam curing revealed this important potential of PC–SF–GGBFS binder system. On the other hand for the granite series, GGBFS behaved well as a silica source for autoclaving. This is also showed that there are some unreacted SF or GGBFS even after autoclaving when the ternary system used and SF can be decreased in mixture designs without mechanical performance loss. Micro-structural investigations was also supported this finding (Fig. 11).

The 28-day strength on standard curing can be achieved in about 24 h with autoclave curing [32]. Nevertheless, there are a few disadvantages to autoclaved products such as the high capital cost of the plant. The bond strength between the concrete and the reinforcement is usually much lower (by about 50%), and the material tends to be more brittle than ordinary concrete after autoclave curing [33]. Under the conditions of high temperature and pressure, the chemistry of hydration is substantially altered. C–S–H forms but is converted to a crystalline product α-calcium silicate hydrate (α-C_2SH) which causes an increase in porosity and reduction in strength. However, in the presence of silica α-C_2SH converts to tobermorite ($C_5S_6H_5$) on continued heating thus high strength can be obtained. On the other hand, prolonged autoclaving may cause the formation of other crystalline calcium silicate hydrates with a strength reduction. It is believed that the complete conversion of amorphous phases to crystalline tobermorite is not desirable and there is an optimum ratio for maximum strength [34–37]. Xi et al. [38] showed that the strength of slag cement also decreases with prolonged autoclaving. However, with a small addition of silica fume, the cement strength increases and the pore structure is densified [38]. For 175 °C hydrothermal curing, the main hydrates of PC-slag cement are α-C–S–H, C–S–H(I) and probably some CAS_2H_4. In addition, silica fume particles fill micro and sub-micrometer level pores in the paste and limit the particle size of hydrates, which is a space filling effect [39].

The compressive strength of mixtures containing granite aggregate is shown in Fig. 2. Comparing to the Fig. 1, compressive strength of these mixtures is lower than the mixtures containing bauxite in all curing conditions. This finding is possibly related to the strength and microstructure of the aggregate. SEM micrographs revealed the porous and rough structure of sintered bauxite and smooth structure of quartz and granite, which affects the performance of aggregate in RPC possibly due to the mechanical interlocking between paste and aggregate. Note that although it has a porous structure sintered bauxite is a hard and high strength material with high specific gravity (3.24). Furthermore, the main chemical components of aggregates are 29% SiO_2 and 67% Al_2O_3 in bauxite, 68% SiO_2 and 19% Al_2O_3 in granite, 99% SiO_2 in quartz. The compressive strength showed a general trend similar to the bauxite mixtures for granite aggregate RPC. On the other hand the main difference with the bauxite mixtures is the SF content which is important especially for autoclave curing. SF content was constant at 280 kg/m^3 in bauxite mixtures while it was reduced with the increasing GGBFS replacement in granite series; however the SF/PC weight ratio was kept constant at 0.3 in granite mixtures. In other words, GGBFS is used as a fine silica source in granite containing mixtures. As can be seen in Fig. 2, decreasing SF content and increasing GGBFS replacement also increased the compressive strength under autoclaving compared to the control mixture G-S0 which contains only cement and SF. This behavior was similar to the bauxite series containing constant SF contents.

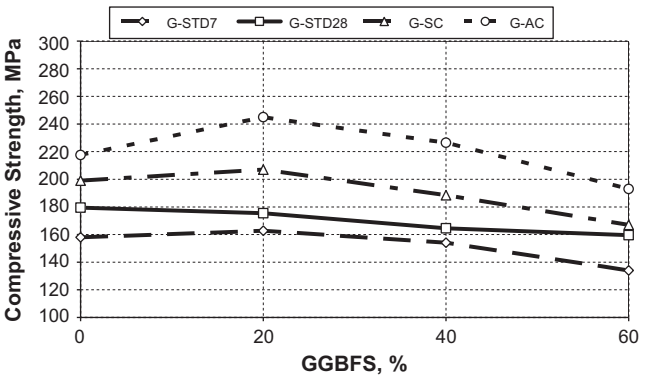

Fig. 2. The influence of GGBFS content on compressive strength of granite aggregate RPC (STD: Standard curing, SC: Steam curing, AC: Autoclave curing).

It must be mentioned that the granite series also included fine quartz as a silica source for autoclaving; however, preliminary tests showed that GGBFS mixtures without fine quartz gave also satisfactory results under autoclaving compared to the Portland cement concrete. Decreasing the SF with GGBFS replacement in RPC mixtures decreased the superplasticizer demand considerably compared to the G-S0 mixture (Table 2).

Furthermore, the maximum aggregate size of RPC mixtures in this study was 3 mm, and 80% of the total aggregate was used as coarse particles (1–3 mm) in all mixtures. In preliminary tests this modification gave good results compared to conventional RPC in which all aggregate is in powder form (<0.1 mm). Richard and Cheyrezy [2,3] suggested the elimination of the coarse aggregate to enhance the homogeneity and used aggregates smaller than <600 μm for RPC200 and <800 μm for RPC800. The results showed that RPC can be produced with coarser aggregate as well as fine aggregate powder. This finding was also reported by Collepardi et al. [11].

3.2. Influence of the blast furnace slag content flexural performance of RPC

Flexural load–deflection curves of autoclaved bauxite mixtures containing different amounts of GGBFS are presented in Fig. 3. GGBFS replacement positively affected the flexural behavior of RPC. The maximum bending loads of all GGBFS mixtures were considerably greater than those of the Portland cement RPC (control). This behavior can be attributed to the improvement in binder phase with GGBFS, which also improves the bond strength between the matrix and the fibers as well as the compressive strength. The displacement at maximum load is between 0.42 and 0.49 mm for all mixtures, and slightly lower for GGBFS mixtures relative to B-S0. After the peak load, gradual load decrement was observed in all series. It can be note that the residual strength at 3 mm displacement was also a significant level. The residual load was over 3000 N at 3 mm displacement and this value increased with increasing GGBFS. High load carrying capacity after the peak load indicates improved toughness and the reinforcing effect of the steel fibers. Similar trends were observed for SC and STD curing conditions, not presented here. Instantaneous load decrements and increments were observed in descending branch of B-S0. This behavior is probably related to the length of fibers, orientation of fibers, gradual pulling out of the fibers and matrix-fiber bond. This behavior is also reported in the literature for ultra-high performance fiber reinforced composites [39]. However, instantaneous drops diminished with GGBFS replacement.

Load–deflection curves of B-S60 mixture after different curing regimes are given in Fig. 4. This figure shows there is a difference between the flexural and compressive behavior of RPC according to the curing conditions. While the compressive strength after AC and SC curing was considerably higher than that of standard curing, after 90 days, the highest flexural strength was obtained for STD curing. The load–displacement relationship of 90-day STD cured samples was similar to that of the AC ones, while the peak load of SC specimens was lower than that of the others. The descending parts of the load–displacement curves are similar but some differences also exist in Fig. 4. The tail of descending branch of STD cured B-S60 showed the instantaneous load decrements and increments.

Load–displacement curves of granite mixtures were presented in Fig. 5. Similar to the bauxite mixtures, instantaneous load decrements and increments were observed in the descending branch of the G-S0 and G-S20 series. This behavior diminished with increasing GGBFS replacement. Maximum flexural strength was observed from G-S20 mixture. The residual load of GGBFS mixtures at 3.0 mm displacement is greater than G-S0.

Fig. 6 shows load–deflection relationship of G-S40 mixture under different curing conditions. Instantaneous load decrements and increments were also observed especially in 7 and 28 days standard cured specimens. This behavior was less obvious with steam and autoclave curing. While, AC cured specimens showed a similar behavior to that of 28-day STD curing, SC curing showed a steam decreased the flexural performance compared to the latter. Resid-

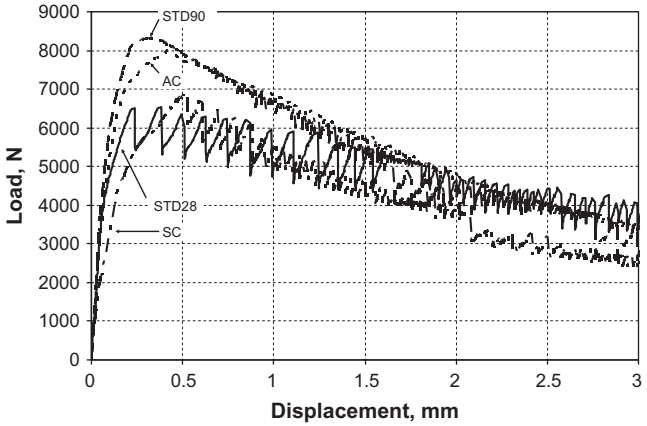

Fig. 4. The Load–displacement relationship of B-S60 mixture after different curing conditions (Flexural loading, Testing ages: STD28-28 days; STD90-90 days; SC-8 days; AC-2 days).

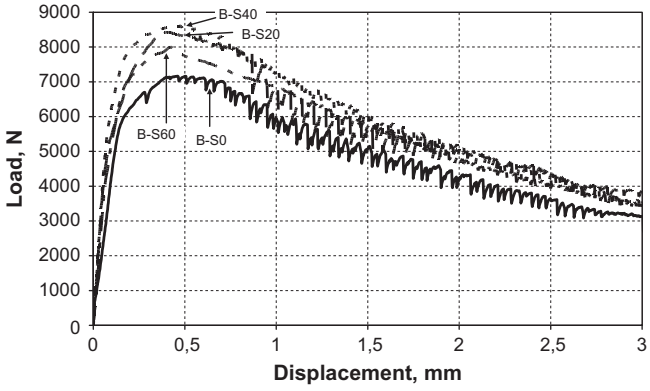

Fig. 3. The load–displacement relationship of autoclaved Bauxite aggregate mixtures according to the GGBFS content (Flexural loading, Testing age: 2 days).

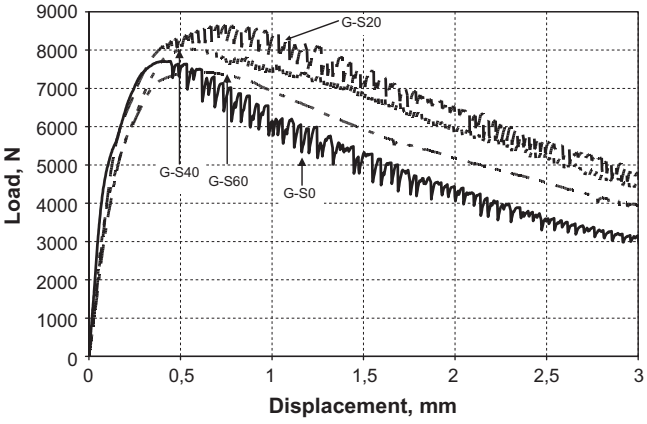

Fig. 5. The Load–displacement relationship of autoclaved Granite aggregate mixtures according to the GGBFS content (Flexural loading, Testing age: 2 days).

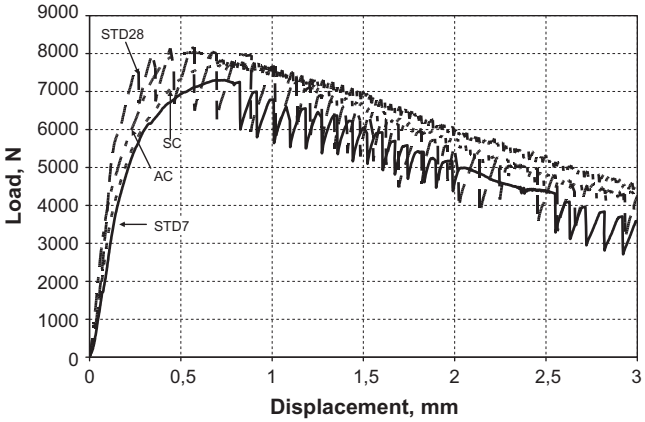

Fig. 6. The Load–displacement relationship of G-S40 mixture after different curing conditions (Flexural loading, Testing ages: STD7-7 days; STD28-28 days; SC-8 days; AC-2 days).

ual load at 3 mm displacement is over 4000 N in all curing conditions except 7-day standard curing.

Flexural strength, toughness and fracture energy values of mixtures after different curing conditions were presented in Table 3. GGBFS replacement generally positively affected the flexural strength, toughness and fracture energy in both bauxite and granite series. This can be attributed to the improvement in bond strength using with GGBFS. Steam curing slightly reduced the flexural strength, toughness and fracture energy compared to the 28-day standard curing. Mechanical properties of autoclaved specimens were greater than 28 days standard cured series. On the other hand, greater flexural strength and fracture energy values were obtained especially at low GGBFS replacement levels after 90 days STD curing compared to the autoclave curing. Although steam and autoclave curing increased the compressive strength significantly, improvement in flexural behavior was not to the same extent. This is probably due to the weaker bond between the fibers and matrix after these curing regimes [32]. Note that reducing the SF with increasing GGBFS replacement in granite series (Table 2) gave also good results compared to the bauxite series (Table 3); this indicates that GGBFS can also be used as a fine silica source especially for autoclaving. Furthermore, it should be emphasized that the flexural strength obtained from the notched beam test may be affected by the stress singularity at the notch [40].

3.3. Influence of pressure application before and during setting on compressive strength of high volume GGBFS RPC

An external pressure can be applied before and during setting to the RPC mixtures to improve the compacted density. Moreover, if the applied pressure is maintained throughout the setting typically for between 6 and 12 h after mixing, part of the porosity appearing in the sample as a result of chemical shrinkage can be eliminated [2]. In this study, a pressure of 30 MPa was applied to the some selected mixtures (B-S0, G-S0, B-S40, B-S60 and G-S40) after casting and this pressure was maintained during 8 h. For this purpose 100 mm × 100 mm special cylindrical steel molds were used. After demolding, the specimens were kept in laboratory atmosphere for 8 h and then autoclaved (2.0 MPa, 210 °C) for 8 h. The compressive strength of the mixtures was determined after cooling; the results are presented in Fig. 7. Design modification in these mixtures (Table 2) was only their SP content which was decreased for the pressure applied series. The SP content of B-S0, BS-40, B-S60, G-S0 and G-S40 reduced to 43, 43, 43, 49 and 33 L/m^3, respectively; this implies a SP saving ratio in mixture design between 20% and 25%. It can be concluded from Fig. 7 that bauxite mixtures showed significantly higher compressive strength than granite mixtures after pressure application process. Compressive strength of RPC reached up to 400 MPa. The performance of high volume GGBFS RPC was more impressive. Note that, the cement content of B-S40 and B-S60 were 576 and 376 kg/m^3, respectively, and compressive strengths were 378 and 320 MPa after pressure application process. Pressure application also increased the compressive strength of the granite series; however, this increment is not as high as in bauxite series. These findings can be attributed to the individual mechanical performance and physical properties of the bauxite and granite. The application of pressure improved the matrix phase ultimately due to the increased compacted density and decreased porosity and it seems that ultra-high strength aggregate is essential under this condition to obtain the RPC400. It is well known that decreasing the water/binder ratio below a certain level is not prac-

Table 3
Flexural performance of the mixtures.

	Bauxite				Granite			
	B-S0	B-S20	B-S40	B-S60	G-S0	G-S20	G-S40	G-S60
	Standard cured, 7 days							
Flexural Strength (MPa)	25.0	28.8	27.3	24.0	23.6	25.0	28.0	25.8
Fracture Energy N/m	4600	5576	5763	4904	4625	5426	5600	5487
Toughness N mm	12,821	15,567	16,092	13,675	12,890	15,143	15,632	15,315
	Standard cured, 28 days							
Flexural strength (MPa)	28.2	29.8	32.1	25.1	29.3	30.0	31.3	30.5
Fracture energy N/m	5411	5716	6183	5281	5358	5526	6155	6095
Toughness N mm	15,102	15,960	17,271	14,735	14,952	15,423	17,194	17,024
	Standard cured, 90 days							
Flexural strength (MPa)	30.0	33.2	32.1	31.5	–	–	–	–
Fracture energy N/m	5920	6161	6205	5835	–	–	–	–
Toughness N mm	16,532	17,210	17,335	16,295	–	–	–	–
	Steam cured							
Flexural strength (MPa)	25.6	27.2	28.2	26.4	26.7	28.0	29.7	27.8
Fracture energy N/m	5020	5338	4782	4569	5261	5920	6330	6110
Toughness N mm	14,002	14,896	13,332	12,732	14,679	16,532	17,686	17,066
	Autoclave cured							
Flexural strength (MPa)	27.5	32.4	33.1	30.7	29.6	33.3	30.8	28.5
Fracture energy N/m	5233	6164	6397	5969	5477	7186	6727	6038
Toughness N mm	14,601	17,219	17,875	16,670	15,287	20,094	18,804	16,866

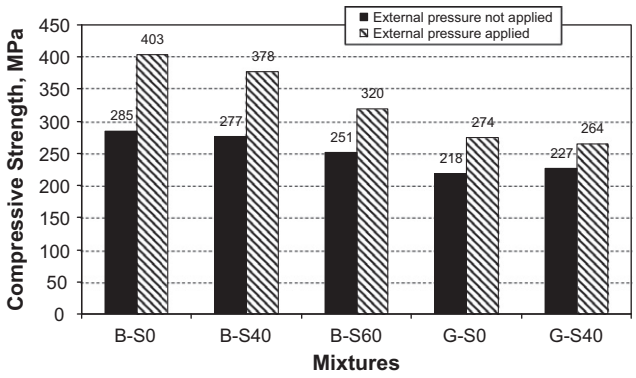

Fig. 7. The effect of pressure application before and during setting on compressive strength.

tical from a mechanical point of view because the strength of the concrete will not significantly exceed the compressive strength of the aggregate. When the compressive strength is limited by the aggregate, the only way to get higher strength is to use a stronger aggregate [41]. Furthermore, it seems that porous structure of sintered bauxite also advantageous especially under pressure, which possibly forced the binder phase to penetrate into the pores. The surface texture of the bauxite aggregate which consist short and thick prismatic needles is shown in Fig. 8a. This rough texture explains the high mechanical performance possibly due to the mechanical interlocking between paste and aggregate especially after pressure application.

3.4. Microstructure of RPC

The microstructure of the selected RPC mixtures was investigated by a using JEOL JSM 6060 electron microscope (SEM). The samples were prepared by taking small pieces from the prismatic specimens. The microstructure and morphology of the RPC were observed on fractured surfaces using with secondary electron imaging. The general micro-structural features of hydrated cement paste can be determined by using backscattered electron (BSE) imaging; however, the resolution of BSE is generally less than secondary electron imaging. The basic principles of BSE imaging of cementitious microstructures were explained by Scrivener [42] and Diamond [43]. Fractured small samples were mounted on the SEM stubs by using carbon paint; the samples were coated with gold. The SEM study was carried out by using an accelerating voltage of 20 kV.

Microstructure investigations revealed the very dense microstructure of RPC. Although the matrix phase of RPC are significantly denser and homogeneous than normal concrete, which indicates very low porosity, entrained or entrapped air pores were also found in the RPC matrix (Figs. 8 and 9). These spherical pores, most of which formed possibly due to the side effect of high amount of superplasticizer, have different diameters in the range of 10–300 μm. These pores generally were empty in standard or steam cured samples however partially filled with tobermorite in autoclaved ones. AC cured B-S0 mixture was shown in Fig. 8b, it can be seen that spherical pores have been partially filled with needle-like tobermorite after autoclaving. Energy dispersive spectroscopy (EDS) analysis showed that Ca/Si, S/Ca and Al/Ca ratios of this type of tobermorite were 1.19, 0.014 and 0.064, respectively. The

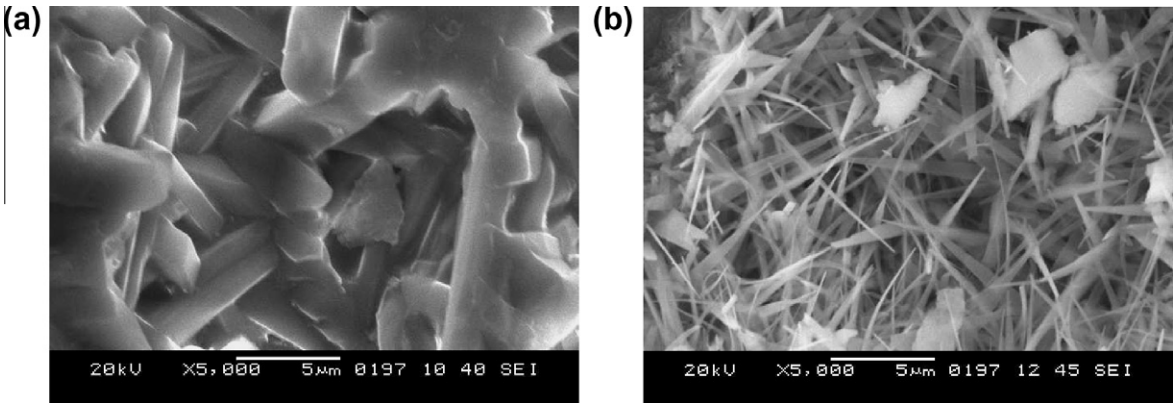

Fig. 8. SEM images of bauxite aggregate and autoclaved B-S0 mixture (a) surface texture of bauxite aggregate (b) spherical pores filled with needle-like tobermorite.

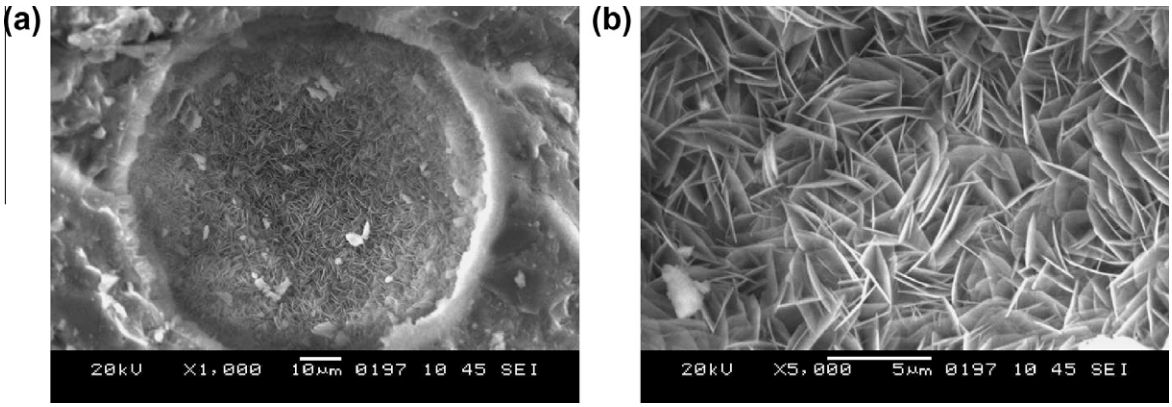

Fig. 9. SEM images of autoclaved B-S60 mixture (a) a spherical pore filled with (rose-like) tobermorite (b) foiled tobermorite in the same pore (higher magnification).

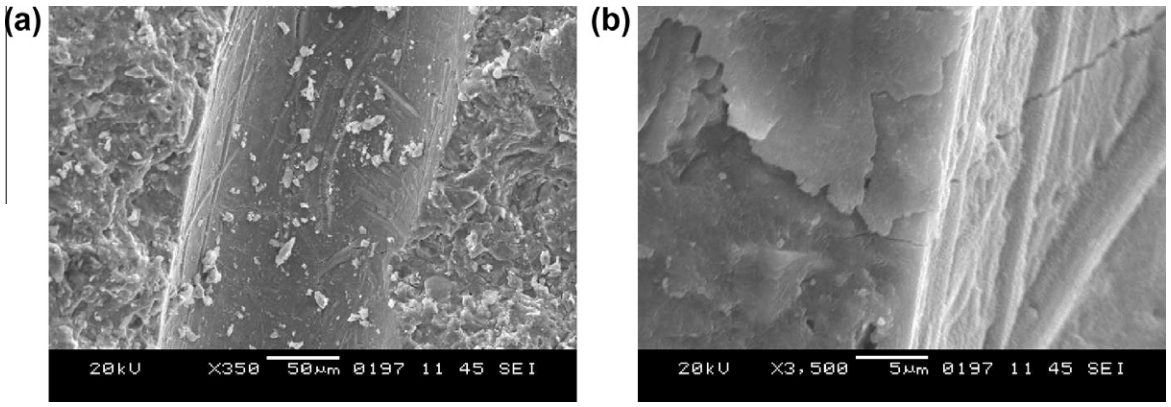

Fig. 10. SEM images of standard cured B-S0 mixture (a) fiber space after fiber pullout (b) transition zone in fiber space.

matrix phase between the spherical pores is very dense. This finding is in accordance with the ultra-high compressive strength of 285 MPa. The binder grains were close to each other due to very low water/binder ratio which causes reduced porosity. Therefore, RPC matrix is very compact and essentially composed of inner hydration products resembling a gel developed through a diffusion process similar to high performance concrete [41].

The microphotographs of autoclaved B-S60 (60% GGBFS replacement) mixture are shown in Fig. 9. Foiled tobermorite was observed in the various spherical pores, one of which is shown in Fig. 9b which is approximately 90 μm in diameter. EDS analysis gave Ca/Si, S/Ca and Al/Ca ratios of 0.65, 0.018 and 0.044, respectively. The matrix phase has also very dense microstructure in the presence of high volume GGBFS. Mostafa [44] also showed different types of tobermorite in autoclaved aerated concrete and reported that in high-lime mixes containing up to 30% air cooled slag, the initially formed fibrous calcium-rich C–S–H changed to needle-like and lath-like 1.1 nm tobermorite.

SEM images of standard cured B-S0 mixture are presented in Fig. 10. The space remaining after fiber pullout from the matrix and surrounding matrix with very low porosity can be seen (Fig. 10a). Moreover, Fig. 10b showed the absence of a visible transition zone between the fiber and dense matrix in accordance with the literature [43].

The general micro-structural features of RPC mixtures were also investigated by using backscattered electron (BSE) imaging. Microstructure investigations revealed the very dense microstructure of RPC due to very low water/binder ratio. As an example, BSE images of autoclaved bauxite aggregated RPC (B-S0 and B-S60) are presented in Fig. 11. Fig. 11a shows fiber (white circular area), bauxite

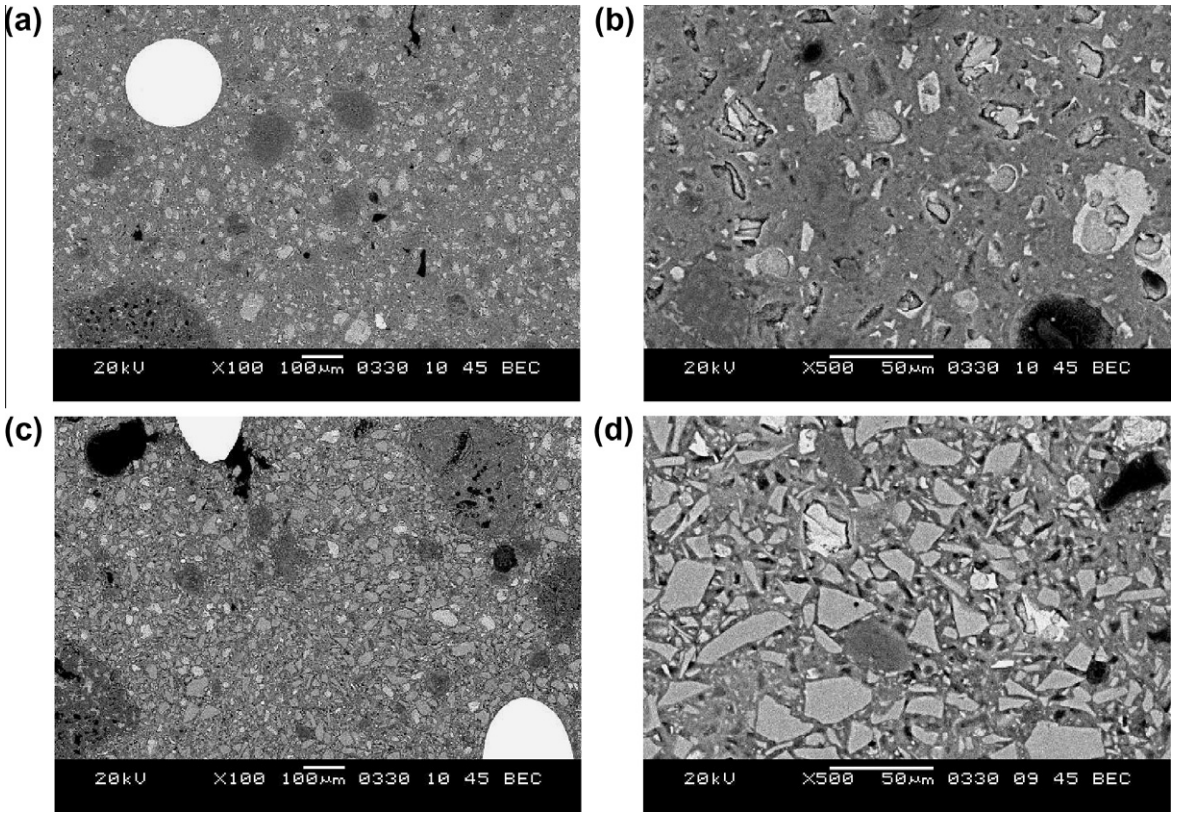

Fig. 11. SEM images of RPC in BSE mode (a) autoclave cured B-S0 mixture (b) micrograph of the B-S0 at higher magnification (c) autoclave cured B-S60 mixture (d) micrograph of the B-S60 at higher magnification.

aggregate (dark grey porous area), pores (black areas), and matrix. As mentioned before, this porous nature of sintered bauxite aggregate provides good mechanical bond with matrix phase. Fig. 11b shows matrix phase of B-S0. The matrix phase predominantly consists of outer product. There are a large number of small grains in these areas which have been termed undesignated product or groundmass. There is considerable infilling of the large capillary pores by this undifferentiated product during hydration [42]. Unhydrated cement grains also exist (light grey areas in Fig. 11a and b). There are spherical pores in RPC one of which is visible at the bottom of Fig. 11b. Similar dense microstructure is also visible for slag incorporated RPC (Fig. 11c and d). Slag grains can be seen in Fig. 11d as sharply angular in accordance with literature [22]. Although a major part of the slag grains is unhydrated, especially for the larger grains, these mixtures have great mechanical performance after autoclave curing. This can be attributed the CH consumption of the SF and slag which needs the CH to form C–S–H [20–22]. In the ternary system (PC–SF–GGBFS) the amount of PC is relatively low and the CH produced would be insufficient to react with all of the SF and GGBFS. Therefore, SF was reduced with increasing GGBFS content in granite series which also showed good mechanical performance. Furthermore, some very dark areas are also visible in Fig. 11. These voids are probably from cement, slag or aggregate grains pulled out during the cutting and polishing stages [22].

4. Conclusions

Test results indicate that production of RPC containing high volume GGBFS is possible both with granite or bauxite aggregates. The compressive strengths of autoclaved granite aggregate RPC containing 40% slag (G-S40) and bauxite aggregate RPC containing 60% slag (B-S60) mixtures are 210 MPa and 254 MPa, respectively. The cement contents of these mixtures are 564 and 376 kg/m^3, which are considerably lower than the cement content of conventional RPC (800–1000 kg/m^3). Besides the reduced heat of hydration and shrinkage, these mixtures have also important environmental and economical benefits.

Silica fume content can be decreased with increasing GGBFS replacement. Moreover, this modification reduced the superplasticizer demand considerably.

Test results revealed that RPC can be produced with 1–3 mm coarse aggregate as well as with aggregate in powder form. Compared to the conventional RPC (aggregate size <0.1 mm), this modification reduces cement and SP demand and also reduces shrinkage.

The compressive strength of RPC can be improved considerably with autoclave or steam curing. This can be attributed to the improvement of hydration process under low pressure steam and high pressure steam curing. On the other hand, steam curing caused some reduction in flexural strength compared to the 28-day standard curing. Furthermore, flexural strength of 90-day standard cured RPC is also more than that of autoclaved RPC, probably due to the decreasing bond strength between matrix and fibers after autoclaving or steam curing, which is important for flexural performance.

Although bauxite aggregate gave higher mechanical performance compared to the granite series, this difference is more pronounced after external pressure application during setting and hardening period. In such case, the compressive strength of RPC reached 400 MPa in the bauxite series compared to 300 MPa in the granite aggregate series. SP content of pressure-applied mixtures can be reduced by a significant amount (20–25%).

SEM investigations revealed the highly dense microstructure of RPC. Furthermore, foiled and needle-like tobermorite with low C/S ratio were identified in autoclaved RPC.

Acknowledgements

This study was supported by the Scientific and Technological Research Council of Turkey (TÜBİTAK, Project No: 104I085). The authors gratefully acknowledge the support of TÜBİTAK. In addition, the authors thank Mr. Mehmet YERLİKAYA from BEKSA-DRA-MIX, Mr. Okan DUYAR and Mr. Osman TEZEL from BASF-YKS and Mrs. Selma CESUR from KARÇİMSA for supplying materials.

References

[1] Bonneau O, Vernet C, Moranville M, Aitcin PC. Characterization of the granular packing and percolation threshold of reactive powder concrete. Cem Concr Res 2000;30:1861–7.
[2] Richard P, Cheyrezy M. Composition of reactive powder concretes. Cem Concr Res 1995;25:1501–11.
[3] Richard P, Cheyrezy MH. Reactive powder concretes with high ductility and 200–800 MPa compressive strength. ACI SP144-24 1994;144:507–18.
[4] Long G, Wang X, Xie Y. Very high-performance concrete with ultrafine powders. Cem Concr Res 2002;32:601–5.
[5] Krönlöf A. Effect of very fine aggregate on concrete strength. Mater Struct 1994;27:185–94.
[6] Song HW, Saraswathy V. Studies on the corrosion resistance of reinforced steel in concrete with ground granulated blast-furnace slag – an overview. J Hazard Mater 2006;138:226–33.
[7] Wang K, Zhi G. Evaluating properties of blended cements for concrete pavements. Final report. Center for Portland Cement Concrete Pavement Technology. Iowa State University; 2003.
[8] Macphee DE, Cao HT. Theoretical description of impact of blast furnace slag on steel passivation in concrete. Mag Concr Res 1993;45:63–9.
[9] Detwiler RJ, Fapohunda CA, Natale J. Use of supplementary cementing materials to increase the resistance to chloride ion penetration of concretes cured at elevated temperatures. ACI Mater J 1994;91:63–6.
[10] Hooton RD, Titherington MP. Chloride resistance of high-performance concretes accelerated curing. Cem Concr Res 2004;34:1561–7.
[11] Collepardi S, Coppola L, Troli R, Collepardi M. Mechanical properties of modified reactive powder concrete. In: Proceedings of the fifth CANMET/ACI international conference on superplasticizers and other chemical admixtures in concrete, SP-173; 1997. pp. 1–21.
[12] Massidda L, Sanna U, Cocco E, Meloni P. High pressure steam curing of reactive-powder mortars. ACI SP200-27 2001;200:447–64.
[13] Shaheen E, Shrive N. Optimization of mechanical properties and durability of reactive powder concrete. ACI Mater J 2006;103:444–51.
[14] Talebinejad I, Bassam SA, Iranmanesh A, Shekarchizadeh M. Optimizing mix proportions of normal weight reactive powder concrete with strengths of 200–350 MPa. In: Ultra high performance concrete (UHPC), international symposium on ultra high performance concrete; September 13–15 2004. pp. 133–41.
[15] Ma J, Orgass M, Dehn F, Schmidt D, Tue NV. Comparative investigations on ultra-high performance concrete with and without coarse aggregates. In: Ultra high performance concrete (UHPC). International symposium on ultra high performance concrete, September 13–15 2004. pp. 205–12.
[16] Rougeau P, Borys B. Ultra high performance concrete with ultrafine particles other than silica fume. In: Ultra high performance concrete (UHPC). International symposium on ultra high performance concrete, September 13–15 2004. pp. 213–25.
[17] Jooss M, Reinhardt HW. Permeability and diffusivity of concrete as function of temperature. Cem Concr Res 2002;32:1497–504.
[18] Gutteridge WA, Dalziel JA. Filler cement: the effect of the secondary component on the hydration of Portland cement Part 2: fine hydraulic binders. Cem Concr Res 1990;20:853–61.
[19] Escalante-Garcia JI. Nonevaporable water from neat OPC and replacement materials in composite cements hydrated at different temperatures. Cem Concr Res 2003;33:1883–8.
[20] Escalante-Garcia JI, Sharp JH. Effect of temperature on the hydration of the main clinker phases in Portland cements: part II, blended cements. Cem Concr Res 1998;28:1259–74.
[21] Gutteridge WA, Dalziel JA. Hydration of Portland cement part I, a fine non-hydraulic filler. Cem Concr Res 1990;20:778–82.
[22] Escalante-Garcia JI, Sharp JH. The microstructure and mechanical properties of blended cements hydrated at various temperatures. Cem Concr Res 2001;31:695–702.
[23] Yazıcı H. The effect of curing conditions on compressive strength of ultra high strength concrete with high volume mineral admixtures. Build Environ 2007;42:2083–9.
[24] Arya C, Xu Y. Effect of cement type on chloride binding and corrosion of steel in concrete. Cem Concr Res 1995;25:893–902.
[25] Glass GK, Reddy B, Buenfeld NR. Corrosion inhibition in concrete arising from its acid neutralization capacity. Corros Sci 2000;42:1587–98.
[26] Basheer PAM, Gilleece PRV, Long AE, McCarter WJ. Monitoring electrical resistance of concretes containing alternative cementitious materials to assess their resistance to chloride penetration. Cem Concr Compos 2002;24:437–49.

[27] Pal SC, Mukherjee A, Pathak SR. Investigation of hydraulic activity of ground granulated blast furnace slag in concrete. Cem Concr Res 2003;33:1481–6.
[28] Bosch VDV. Performance of mortar specimens in chemical and accelerated marine exposure. Perform Concr Mar Environ. 1980;ACI SP-65:487–507.
[29] Roy DM, Idorn GM. Hydration, structure and properties of blast furnace slag cements, mortars and concrete. ACI J 1982;6:44–57.
[30] Toutanji AH, Bayasi Z. Effect of curing procedures on properties of silica fume concrete. Cem Concr Res 1999;29:497–501.
[31] Wu DS, Peng YN. The macro- and micro properties of cement pastes with silica-rich materials cured by wet-mixed steaming injection. Cem Concr Res 2003;33:1331–45.
[32] Neville AM. Properties of concrete. New York: Longman; 1995.
[33] Mindess S, Young JF, Darwin D. Concrete. New Jersey: Pearson Education; 2002.
[34] Aldea CM, Young F, Wang K, Shah SP. Effects of curing conditions on properties of concrete using slag replacement. Cem Concr Res 2000;30:465–72.
[35] Shi C, Hu S. Cementitious properties of ladle slag fines under autoclave curing conditions. Cem Concr Res 2003;33:1851–6.
[36] Glasser FP, Hong SY. Thermal treatment of C–S–H gel at 1 bar H_2O pressure up to 200 °C. Cem Concr Res 2003;33:271–9.
[37] Yang Q, Zhang S, Huang S, He Y. Effect of ground quartz sand on properties of high-strength concrete in the steam-autoclaved curing. Cem Concr Res 2000;30:1993–8.
[38] Xi Y, Siemer DD, Scheetz BE. Strength development, hydration reaction and pore structure of autoclaved slag cement with added silica fume. Cem Concr Res 1997;27:75–82.
[39] Maeder U, Gamboa IL, Chaigmon J, Lombard JP. Ceracem, a new high performance concrete: characterizations and applications. In: Ultra high performance concrete (UHPC), International symposium on ultra high performance concrete September 13–15 2004. pp. 59–68.
[40] Wong YL, Lam L, Poon CS, Zhou FP. Properties of fly ash-modified cement mortar-aggregate interfaces. Cem Concr Res 1999;29:1905–13.
[41] Aitcin PC. The durability characteristics of high performance concrete: a review. Cem Concr Compos 2003;25:409–20.
[42] Scrivener KL. Backscattered electron imaging of cementitious microstructures: understanding and quantification. Cem Concr Compos 2004;26:935–45.
[43] Diamond S. The microstructure of cement paste and concrete-a visual primer. Cem Concr Compos 2004;26:919–33.
[44] Mostafa NY. Influence of air-cooled slag on physicochemical properties of autoclaved aerated concrete. Cem Concr Res 2005;35:1349–57.